Journal of Alloys and Compounds 695 (2017) 656–667

Contents lists available at ScienceDirect

Journal of Alloys and Compounds

journal homepage: http://www.elsevier.com/locate/jalcom

Modelling the sulfate capacity of simulated radioactive waste borosilicate glasses

P.A. Bingham [a, *], S. Vaishnav [a], S.D. Forder [a], A. Scrimshire [a], B. Jaganathan [a], J. Rohini [a], J.C. Marra [b], K.M. Fox [b], E.M. Pierce [c], P. Workman [b], J.D. Vienna [d]

[a] Materials and Engineering Research Institute, Sheffield Hallam University, Howard Street, Sheffield S1 1WB, UK
[b] Savannah River National Laboratory, Savannah River Site, 999-W, Aiken, SC 29808, USA
[c] Oak Ridge National Lab, Biological and Environmental Science Directorate, Oak Ridge, TN 37831, USA
[d] Pacific Northwest National Laboratory, Nuclear Sciences Division, Richland, WA 99352, USA

ARTICLE INFO

Article history:
Received 3 September 2016
Received in revised form
20 October 2016
Accepted 8 November 2016
Available online 10 November 2016

Keywords:
Borosilicate
Glass
Sulfate
Capacity
Waste
Radioactive

ABSTRACT

The capacity of simulated high-level radioactive waste borosilicate glasses to incorporate sulfate has been studied as a function of glass composition. Combined Raman, ^{57}Fe Mössbauer and literature evidence supports the attribution of coordination numbers and oxidation states of constituent cations for the purposes of modelling, and results confirm the validity of correlating sulfate incorporation in multi-component borosilicate radioactive waste glasses with different models. A strong compositional dependency is observed and this can be described by an inverse linear relationship between incorporated sulfate (mol% SO_4^{2-}) and total cation field strength index of the glass, $\Sigma(z/a^2)$, with a high goodness-of-fit ($R^2 \approx 0.950$). Similar relationships are also obtained if theoretical optical basicity, Λ_{th} ($R^2 \approx 0.930$) or non-bridging oxygen per tetrahedron ratio, NBO/T ($R^2 \approx 0.919$), are used. Results support the application of these models, and in particular $\Sigma(z/a^2)$, as predictive tools to aid the development of new glass compositions with enhanced sulfate capacities.

1. Introduction

Sulfur can be a problematic component of certain civil and defence radioactive wastes that are destined to be converted into wasteforms by vitrification. Such sulfur-bearing wastes include, but are not limited to, waste liquors arising from the PUREX process [1,2] and spent ion exchange resins [3]. The presence of sulfur can pose problems for safe, cost-effective waste vitrification due to its low (<ca.1 wt% SO_3) capacity in the alkali borosilicate glasses that are used globally as radioactive waste host matrices [3–10]. Sulfate capacity is defined for the purposes of this study as the non-equilibrium sulfate solubility, i.e. the sulfate solubility as determined under a set of consistent non-equilibrium conditions, as arise in most laboratory-scale and industrial-scale glass melting operations. If the sulfate capacity limit of an oxide glass is exceeded during melting, a molten salt or "gall" layer forms on the melt surface. This is highly undesirable for several reasons. Radionuclides such as ^{135,137}Cs, ^{99}Tc and ^{90}Sr migrate into this water-soluble sulfate layer during melting [4,6,9,10] and the salt layer can thereby provide a pathway for these radionuclides to readily be released into the environment following contact with water in a geological waste repository. In addition, molten salts can affect processing of the waste: they exhibit low viscosities and their high corrosivities toward melt vessels shorten melter service lifetimes [4,6,9,10]. Consequently, research has focussed on optimising sulfate incorporation levels and establishing melter operating parameters that maintain sulfate levels below their capacity limit in the glass melt [6,9–15]. This, in turn, can restrict the types and concentrations of waste that can be vitrified, ultimately increasing the costs and timescales associated with waste vitrification, interim storage and final geological disposal.

Development of new or modified glass compositions with enhanced sulfate capacities remains a global research priority. Indian scientists have developed SiO_2-B_2O_3-Na_2O-BaO and SiO_2-B_2O_3-Na_2O-PbO glasses for high-level radioactive waste vitrification [1,16,17], some of which can incorporate up to 3 mol % SO_4^{2-} without formation of a salt layer during melting [16]. This level of sulfate incorporation is considerably higher than accepted sulfate capacities in traditional alkali borosilicate glasses, which are

* Corresponding author.
E-mail address: p.a.bingham@shu.ac.uk (P.A. Bingham).

http://dx.doi.org/10.1016/j.jallcom.2016.11.110
0925-8388/

usually less than 1 mol % SO_4^{2-} [6,9–15]. Although the Indian glasses have been the focus of considerable study (see, for example, [1,16,17]) the origins of their high sulfate capacity are not apparent. One plausible explanation may be that their low (1000 °C) melting temperatures play a role, since lower melting temperatures can enhance the sulfate capacity and solubility in some oxide melts [18–20]. However, other possible explanations also exist and further work is required to explain this behaviour. The Indian results for BaO-containing glasses are commensurate with Ooura and Hanada [21], who demonstrated high (1–3 mol % SO_3) sulfate capacities in BaO-containing SiO_2-Na_2O-BaO glasses and linked the alkaline earth contribution with the thermal decomposition equilibrium constant of its sulfate. Other silicate glasses rich in BaO and exhibiting high sulfur capacities have been developed for vitrification of sulfur-rich spent ion exchange resins [3,7,8]. Generally, literature supports the addition of large, basic, low field strength cations as a means of enhancing sulfate capacities in silicate and borosilicate glasses [3,4,6–8,10,16,17,21]. For other oxide glass systems, P_2O_5-Al_2O_3-Na_2O-Fe_2O_3 glasses exhibiting high sulfate capacities have been used as vitrification matrices at the Russian Mayak facility [2]. Some phosphate glasses can accommodate sulfate contents of the order of several percent [2,4]. However, borosilicate glasses are the global material of choice for the majority of radioactive waste vitrification activities and thus we have focussed here on borosilicate glasses.

Glass composition plays a key role in determining sulfate capacity and solubility [2–21] and the relative concentrations of O^0, O^- and O^{2-} (bridging oxygen, non-bridging oxygen and free oxygen, respectively) are major factors in this [4,6,10,18–21]. A number of research papers and reviews have been published concerning prediction or modelling of the capacity and solubility of sulfate and other anionic species in oxide glasses (see, for example [4,6,10,19,20], and references therein). Any mechanistic-based model, in order to be useful, must include a meaningful representation of glass composition and/or structure; and must be able to accommodate a broad range of chemical elements which may be present in the glass in sufficient concentration to have an impact on sulfur behaviour. A range of numerical scales have been developed which can, to varying degrees, fulfil these requirements. These range from simple scales, for example molar concentration of glass forming oxides ([SiO_2], [P_2O_5], [B_2O_3], [$SiO_2 + B_2O_3$] etc.), to more structurally representative scales such as the ratio of oxygen to glass former ([O]/[Si], [O]/[P] etc.), the ratio of non-bridging oxygen to tetrahedral cations (NBO/T), or the ratio of non-bridging oxygen to bridging oxygen (NBO/BO). However, these scales lack the subtlety to consider, for example, the different effects of chemically similar components, for example, Li_2O and Na_2O or MgO and CaO, or differences in their effects on glass structure (e.g., ionic radii), although in the case of NBO/T this can be accommodated in terms of relative NBO and T contributions. To achieve higher levels of discrimination more detailed scales, with terms for each glass component, are worthy of investigation. This latter category includes the cation field strength and optical basicity scales, which are among the most well-known and widely-utilised of such scales within glass science. Previously, models using these scales were applied to sulfate capacity data for a range of phosphate glasses and a small number of borosilicate glasses [4]. It was observed that cation field strength index, $\Sigma(z/a^2)$ provided the most accurate relationship with sulfate capacity across a wide range of surveyed glass compositions. The aim of the work presented here was to apply and compare the cation field strength index and theoretical optical basicity scales to the study of sulfate capacities in a series of simulated multi-component borosilicate glasses representative of U.S. high-level radioactive waste glasses from the Savannah River Site, but more widely applicable worldwide. It is important to note that the aim of this work was to investigate the inherent capacity of the glasses studied to incorporate sulfate as dissolved species within their atomic structure under imposed near-sulfate-saturation conditions. It is acknowledged that during real-world waste vitrification, conditions are likely to differ from those studied in the laboratory. For example there may be differences in melting temperature, redox conditions, batch or glass compositions that include the presence of other salts (e.g., halides or nitrates), or organics. Any of these factors can influence sulfate capacity and solubility in glass - but the inherent capacity of any glass to incorporate sulfate under a given set of conditions is a function of glass composition and structure, and that is the focus of the work presented here. The goal was to gain improved understanding of the mechanisms controlling sulfate solubility in glasses, and in particular to build a tool that can assist glass scientists and technologists in predicting the inherent capability of radioactive waste borosilicate glasses to incorporate sulfate.

2. Materials and methods

A total of eleven experimental glasses were prepared in two inter-related series, Series A and B, which are broadly representative of U.S. high-level radioactive waste glasses (see, for example, [9,11–15]). Analysed compositions of all glasses are shown in Table 1. Sulfate was added to the batch as Na_2SO_4 at levels providing what was expected to be a modest excess of Na_2SO_4: 2 wt% SO_4^{2-} equivalent was present in each nominal glass composition. All glasses were expected to exhibit sulfate capacities and solubilities below 2 wt% SO_4^{2-} and thus form a sulfate "gall" layer on the surface of the glass melt, enabling sulfate saturation of the molten glass to be achieved, or at the very least, approached. Batches to make 150 g of glass were prepared using appropriate levels of dried sand (purity > 99.9%) and analytical grade raw materials (Li_2CO_3, Na_2CO_3, Na_2SO_4, Fe_2O_3, $Al(OH)_3$, H_3BO_3, $CaCO_3$ and ZrO_2) which were weighed into sample bags using a calibrated balance, then mixed thoroughly to ensure good batch homogeneity. Batches were transferred into a ZrO_2 grain stabilised (ZGS) Pt crucible with a loose-fitting ZGS Pt lid and then placed in an electric furnace at 1150 °C and melted for 1 h. This methodology was selected to enable direct comparison with data previously obtained for simulated U.S. waste glasses [12,13] that were prepared under the same conditions. After 1 h of melting the crucible was removed from the furnace and the molten glass was poured into a steel mould and allowed to cool without annealing. In most cases a sulfate "gall" layer was observed, which indicates that the sulfate capacity-limit of the glass melt was exceeded. These samples were washed for 5 min under running hot water (ca. 50–60 °C) to dissolve and remove excess sulfate salts. Samples were then carefully dried. Glasses were ground to a fine powder and washed in dilute nitric acid to remove any remaining sulfate phases. X-ray diffractometry was performed on all samples using a PANalytical Empyrean X-ray diffractometer and results confirmed that all samples were X-ray amorphous. Samples B1 and B2 were found to contain very minor amounts of crystalline SiO_2, it is believed that this was due to a few grains of undissolved raw material sand which were observed at the glass/air/crucible boundary in these two glass samples, and the errors that this minor amount of undissolved SiO_2 introduced into sulfate capacity modelling have been incorporated in the estimated uncertainties. Two preparation techniques, sodium peroxide fusion and lithium metaborate/tetraborate fusion, were used to prepare the glass samples, in duplicate, for compositional analysis. Solutions ob-

Table 1
Analysed glass compositions (mol%) to 2 d.p. and associated model parameters. Uncertainties are described in Section 2.

Mol%	Al_2O_3	B_2O_3	Fe_2O_3	Li_2O	Na_2O	K_2O	MgO	CaO	MnO	P_2O_5	SiO_2	TiO_2	ZrO_2	SO_4^{2-}	Sum
Glass A1	3.55	4.66	5.47	7.79	10.9	0.17	0.16	6.29	0.05	0.03	59.63	0.02	0.53	0.753	100.00
Glass A2	3.76	7.34	5.86	8.85	11.86	0.06	0.16	6.90	0.05	0.03	53.80	0.01	0.53	0.792	100.00
Glass A3B3	3.93	7.30	6.49	10.89	13.95	0.06	0.16	8.58	0.05	0.03	47.06	0.01	0.63	0.876	100.00
Glass A4	4.11	6.91	6.13	11.85	15.28	0.13	0.59	9.25	0.05	0.03	43.98	0.02	0.68	1.012	100.00
Glass A5	4.96	7.94	5.77	12.79	16.41	0.17	1.13	10.48	0.04	0.04	38.65	0.02	0.66	0.938	100.00
Glass A6	5.01	7.71	6.41	13.81	17.85	0.15	1.06	11.14	0.04	0.04	35.02	0.02	0.71	1.019	100.00
Glass B1	3.98	7.42	4.48	9.89	6.09	0.12	0.81	5.22	0.03	0.03	60.64	0.02	0.60	0.657	100.00
Glass B2	4.02	7.24	4.64	10.15	9.70	0.12	0.85	6.47	0.03	0.03	55.42	0.02	0.62	0.692	100.00
Glass B4	4.15	7.62	4.85	10.53	17.26	0.12	0.93	10.84	0.04	0.03	41.93	0.02	0.64	1.031	100.00
Glass B5	3.89	6.34	4.57	10.43	20.68	0.20	0.91	12.20	0.04	0.03	38.91	0.02	0.62	1.173	100.00
Glass B6	4.04	7.87	4.57	10.27	23.66	0.18	0.90	14.02	0.04	0.03	32.61	0.02	0.62	1.177	100.00
z	3	3	3	1	1	1	2	2	2	5	4	4	4	–	–
CN	4	3.33	4	4	6	8	4	6	5	4	4	5	6	–	–
r/pm	0.39	0.043	0.49	0.59	1.02	1.51	0.57	1	0.745	0.17	0.26	0.5125	0.72	–	–
a/pm	1.77	1.423	1.87	1.97	2.40	2.89	1.95	2.38	2.125	1.55	1.64	1.8925	2.10	–	–
z/a^2	0.9576	1.4856	0.8579	0.2577	0.1736	0.1197	0.5260	0.3531	0.4451	2.0812	1.4872	1.1249	0.9070	–	–
Oxide Λ_{th}	0.61	0.447	0.66	0.81	1.10	1.40	0.51	1.00	0.84	0.47	0.48	0.71	0.72	–	–

tained from each of the prepared samples were analysed by Inductively Coupled Plasma – Optical Emission Spectroscopy (ICP-OES) [22]. The duplicate analyses were averaged to provide a single value for each component. A reference material (LRM) was also analysed for quality control [22]. ICP-OES analysis provided Al_2O_3, B_2O_3, CaO, Fe_2O_3, Li_2O, Na_2O, SO_4^{2-}, SiO_2 and ZrO_2 contents. Further analysis was conducted using X-Ray Fluorescence (XRF) spectroscopy with a Philips MagiXPRO spectrometer. The XRF analyses were conducted using a Wide Range Oxide program and samples were prepared by fusion with lithium tetraborate. Given the greater accuracy of the ICP-OES technique the contents of Al_2O_3, B_2O_3, CaO, Fe_2O_3, Li_2O, Na_2O, SO_4^{2-}, SiO_2 and ZrO_2 listed in Table 1 originate from the ICP-OES analyses. The contents of MgO, K_2O, P_2O_5, MnO and TiO_2 were obtained from the XRF analysis and these constituents presumably originated from raw material impurities. A conservative estimate of errors associated with ICP-OES analyses is ±1% of the measured concentrations. Uncertainties associated with the XRF analyses that have been used to augment the ICP-OES data are larger, owing to the nature of the technique, and are estimated at ±2% of the measured concentrations. All analysed compositions were obtained in weight % then converted to molar %. These data, used in Cation Field Strength Index and Optical Basicity calculations, were not rounded, although the analysed compositions presented in Table 1 have been rounded to 2 d.p. for ease of viewing. Further uncertainties are associated with the Cation Field Strength Index model, which requires assumptions for the average coordination of certain cations in glass, and in some cases average coordination can change as a function of glass composition. The uncertainties associated with SO_4^{2-} content are of the greatest importance to this study. The method by which the glasses were prepared may itself have introduced additional uncertainties. The method used, i.e. deliberately saturating the glass melt with sulfate, then cooling and removing any undissolved sulfate via aqueous solution and acid washing, may be imperfect, as indeed are all melt saturation methods. As recently reported [23], the method of preparing sulfate-doped, simulated radioactive waste glasses is robust in terms of approaching the sulfate solubility limit of a given glass composition prepared under atmospheric conditions. True sulfate saturation was achieved in Ref. [23] when the glass and salt were ground and melted 3 times, and gave the best known representation of true sulfate solubility in radioactive waste-type glasses. On the basis of [23] it is reasonable to expect that the sulfate solubility limit of the melts considered here was at least approached and is consistent with previously reported data (e.g., [9–15]). A conservative estimate of uncertainty in (mol %) SO_4^{2-} content in the glasses considered in this study is ±5% of measured value.

2.1. Composition - structure parameters for modelling

The cation field strength index method parameterises glass composition and structure by summation of the field strength contributions from each oxide constituent in a given coordination using the cation field strengths developed by Dietzel [24,25]. In an earlier application of cation field strength modelling to sulfate capacity in radioactive waste glasses, $\Sigma(z/a^2)$, the sum of the cation field strengths of cations in the glass was normalised to 1-mol-cation [4]. Since that work was published the present authors have found that applying total cation field strength index (this is not normalised to 1-mol-cation but normalised only to 1 mol of oxide), and excluding sulfate from the calculation, provides clearer relationships as reflected in values of R^2, and consequently the total cation field strength index has been used in the present work. Sulfate is excluded from the calculation because including it in the calculated value would obscure the ability of a glass to incorporate it.

In order to more clearly understand any structural changes through each series of glasses studied here, and the impact that these changes might have on sulfate capacity and -solubility, structural analyses were carried out. In studies of glasses with low contents (≪1%) of paramagnetic ions such as Fe^{3+}, the speciation of Si-O groups and the B-O and Al-O coordination can readily be studied using MAS-NMR. However, all glasses studied here contain substantial levels of Fe^{3+} which causes paramagnetic broadening of the NMR signal, thus the accuracy of any data extracted is compromised [26,27]. We carried out ^{11}B, ^{27}Al and ^{29}Si MAS-NMR of one sample, A3B3. However, strong paramagnetic broadening occurred as expected, and the results could not be used. Consequently, further MAS-NMR of our glasses was not attempted. Here, ^{57}Fe Mössbauer and Raman spectroscopies have been used to obtain structural information on candidate glasses. This has been combined with information on the most relevant compositions from the substantive body of literature available, in order to provide the most accurate achievable input data on cation coordination and oxidation state for modelling cation field strength and optical basicity values.

Following consultation of a range of structural studies on borosilicate glasses and melts that are compositionally similar to

those studied here, the cation oxidation states and average coordination numbers in our current models have been estimated as follows: $^{[4]}P^{5+}$, $^{[4]}Si^{4+}$, $^{[3.33]}B^{3+}$, $^{[4]}Al^{3+}$, $^{[4]}Fe^{3+}$, $^{[4]}Li^{+}$, $^{[6]}Na^{+}$, $^{[8]}K^{+}$, $^{[4]}Mg^{2+}$, $^{[6]}Ca^{2+}$, $^{[6]}Zr^{4+}$, $^{[5]}Mn^{2+}$, $^{[5]}Ti^{4+}$, $^{[4]}S^{6+}$. A rationale and references supporting these selections is given here, and further support from Raman and ^{57}Fe Mossbauer spectroscopy is provided in the Results and Discussion. P^{5+} and Si^{4+} are known to be 4-fold coordinated with respect to O^{2-} in most oxide glasses [28]. Na^{+} has been shown spectroscopically to be 6-fold coordinated [28,29]; Li^{+} 4-fold coordinated but network-modifying and not network-forming [28–30]; and Ca^{2+} 6-fold coordinated [28,29] with respect to O^{2-} in oxide glasses, although there is spread in the available data, some of which is associated with uncertainties of the techniques used (e.g., X-Ray absorption spectroscopy, neutron diffraction, MAS-NMR). Boron can be $^{[3]}B^{3+}$ and $^{[4]}B^{3+}$ in borosilicate glasses, and the ratio $^{[3]}B^{3+}/^{[4]}B^{3+}$ is normally obtained for glasses using ^{11}B MAS-NMR, although B *K*-edge X-Ray absorption spectroscopy or EELS have also been used. Many authors cite the Yun-Dell-Bray model [31,32] for boron coordination in oxide glasses and this model has been refined and applied to different glasses over the years, including borosilicate glasses [33]. Evidence from studies of broadly similar compositional ranges to those studied here [27,34–37] was used to inform our assumed $^{[3]}B^{3+}/^{[4]}B^{3+}$ ratio to provide an average cation field strength and inform NBO/T for modelling. In terms of the Yun-Dell-Bray model [31,32] parameters R (where R = alkali oxide/B_2O_3) and K (where K = SiO_2/B_2O_3), calculations of R and K for our analysed glasses provide R~4 and K~4.5 to 13, which are beyond the ranges of most compositions studied using the Yun-Bray-Dell model. Moreover, the compositional and structural complexity of our glasses, including the presence of the other tetrahedrally-coordinated species such as $^{[4]}Al^{3+}$ and $^{[4]}Fe^{3+}$ which require alkali cations for charge balance, make estimation of boron coordination on the basis of the Yun-Dell-Bray model even more problematic. Consequently we have not applied the Yun-Dell-Bray model here. Using evidence from Raman spectroscopy (see Discussion) which confirms the presence of $^{[3]}B^{3+}$ as a major proportion of total boron, combined with literature evidence for broadly similar glasses [27,34–37], the boron is estimated to occur in our glasses approximately as follows: 2/3 $^{[3]}B^{3+}$ and 1/3 $^{[4]}B^{3+}$, giving an average of $^{[3.33]}B^{3+}$. There are indications from Raman spectroscopy that average boron coordination may change across the range of samples studied. Consequently our estimation of $^{[3]}B^{3+}/^{[4]}B^{3+}$ carries some uncertainty. However, the low boron contents (<8 mol% B_2O_3) of these glasses mean that the effects of any differences in boron coordination on modelled cation field strength values and on NBO/T used in modelling will be small. However, we have ensured that possible variations in average boron coordination are accommodated in the stated uncertainties used in modelling cation field strength indices, optical basicities and NBO/T.

The outcomes from investigation of selected glasses by ^{57}Fe Mössbauer spectroscopy are discussed in the Results and Discussion sections, and confirm that the iron in the glasses studied here can be considered to all be present as $^{[4]}Fe^{3+}$. Evidence from a number of sources indicates that the Al^{3+} will occur predominantly as $^{[4]}Al^{3+}$ [27,33–38]. Manganese is readily reduced from Mn^{3+} to Mn^{2+} in glasses prepared under oxidising melting conditions, according to electrochemical series [39]. McKeown et al. [40] also demonstrated that Mn^{2+} is the dominant oxidation state in a wide range of US radioactive waste glasses similar in composition to those under consideration here. Therefore, it is reasonable to assume that all Mn is present as Mn^{2+} in the glasses studied here. McKeown et al. [40] also determined that the average coordination of Mn^{2+} in radioactive waste borosilicate glasses is approximately 5, therefore it is assumed for our models that Mn is present as 50% $^{[4]}Mn^{2+}$ and 50% $^{[6]}Mn^{2+}$, in order to obtain an average of $^{[5]}Mn^{2+}$. Magnesium is known to occur largely as $^{[4]}Mg^{2+}$ in the majority of alkali-bearing silicate glasses [29,41,42]. We have assumed $^{[4]}Mg^{2+}$ for our model and applied it to all glasses studied here. Electrochemical series show that titanium is expected to occur in oxide glasses produced under oxidising conditions entirely as Ti^{4+} [39]. Coordination of Ti^{4+} in oxide glasses has been studied extensively by Farges and colleagues [43–45], who concluded that Ti^{4+} occurs predominantly as $^{[5]}Ti^{4+}$ in a wide range of oxide glasses. We have therefore assumed for our models that Ti^{4+} occurs as 50% $^{[4]}Ti^{4+}$ and 50% $^{[6]}Ti^{4+}$ in order to obtain an average of $^{[5]}Ti^{4+}$, in the glasses studied here. For manganese, magnesium and titanium, their low concentrations mean that any changes in oxidation state or coordination from those assumed for modelling, have minimal effects. Zirconium has been shown [46,47] to occur predominantly as $^{[6]}Zr^{4+}$ in oxide glasses broadly similar to those under consideration here, and consequently we have assumed $^{[6]}Zr^{4+}$ in our models.

Finally, it is important to consider oxygen coordination in the glasses studied, for the purposes of calculating cation field strength indices. In a previous publication [4] it was assumed that the average oxygen coordination was 2, as in pure SiO_2. Here we have applied a more realistic average oxygen CN = 4 for oxide glasses, based on the work of Mountjoy [48] and references therein. This approach possibly overestimates average oxygen coordination to network formers and may underestimate average oxygen coordination to network modifiers. Nevertheless, this approach was the most appropriate, based on literature, and it enhances accuracy for calculating cation field strength indices compared with using average oxygen CN = 2.

The above assumptions all carry uncertainties when applied across any range of glass compositions - and some level of variation in coordination and bond lengths can reasonably be expected to arise with changing glass composition. Consequently, these factors have been taken into consideration when estimating uncertainties in our models. A full and detailed structural analysis of each and every glass considered during compositional development would have been time-consuming and expensive, and is unnecessary, provided that sufficient support is available in literature for the assignment of coordination numbers and oxidation states. We have used such an approach here. Total cation field strength index for each glass was calculated according to (1).

$$CFSI_{Total} = \sum_{i=1}^{n}\left(m_i c_i \left(z/a^2\right)_i\right) \quad (1)$$

where m_i = mole fraction of the *i*th oxide; c_i = number of cations in one formula unit of the *i*th oxide; z = cationic valence; and a = interatomic distance in picometers (e.g., the sum of the ionic radius of the cation and the O^{2-} ion). Values of $(z/a^2)_i$ were calculated for the *i*th oxide in the glass. Shannon ionic radii for ions in aqueous solutions [49] were used in all calculations. Fig. 1 shows retained sulfate as a function of $\Sigma(z/a^2)$.

Theoretical optical basicity, Λ_{th}, was calculated for each glass according to the method described by Duffy and Ingram [50]. Updated oxide basicity values were also discussed by Lebouteiller and Courtine [51] and Duffy [52–54]. Oxide basicity values used in our calculations have been selected from these references [50–54], based on the most appropriate value for each constituent considering the oxidation state and average coordination numbers discussed earlier in this section. Parameters used in $\Sigma(z/a^2)$ and Λ_{th} calculations are given in Table 1. Fig. 2 shows retained sulfate as a function of theoretical optical basicity, Λ_{th}.

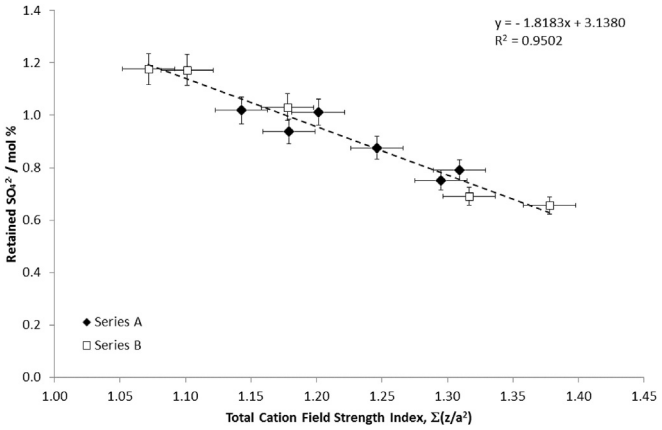

Fig. 1. Retained sulfate, SO_4^{2-}, as a function of total cation field strength index, $\Sigma(z/a^2)$ (excluding sulfate), for model glasses.

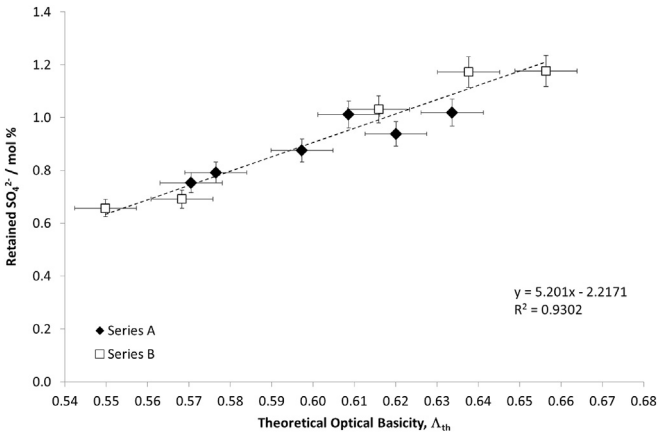

Fig. 2. Retained sulfate, SO_4^{2-}, as a function of theoretical optical basicity, Λ_{th} (excluding sulfate), for model glasses.

The ratio of non-bridging oxygen to tetrahedral cations (NBO_T) was calculated here for each glass according to (2):

$$\frac{NBO}{T} = \frac{2[R_2O] + 2f_M[R'O] + 2f_M[R''O_2] - 2[Al_2O_3] - 2f_T[B_2O_3] - 2f_T[Fe_2O_3]}{[SiO_2] + 2[P_2O_5] + 2[Al_2O_3] + f_T[R'O] + f_T[R''O_2] + 2f_T[B_2O_3] + 2f_T[Fe_2O_3]} \quad (2)$$

where R_2O = Li_2O, Na_2O and K_2O; R'O = MgO, CaO and MnO; $R''O_2$ = TiO_2 and ZrO_2; and where f_T is the fraction of tetrahedrally-coordinated species and f_M is the fraction of glass modifier species (such that $f_T = 1\text{-}f_M$). As discussed earlier in this section, we have assumed the following: Li_2O, Na_2O, K_2O, CaO and ZrO_2 are glass modifiers (i.e. $f_M = 1.0$); and f_T (MgO) = 1.0; f_T (MnO) = 0.5; f_T (B_2O_3) = 0.3333; f_T (Fe_2O_3) = 1.0; and f_T (TiO_2) = 0.5. Fig. 3 shows retained sulfate as a function of calculated NBO/T.

Room temperature ^{57}Fe Mössbauer spectra were collected for end-member glasses A1, A6, B1 and B6, relative to α-Fe over a velocity range of ±6 mm s^{-1} using a constant acceleration spectrometer with a 25 mCi source of ^{57}Co in Rh. Three broadened Lorentzian paramagnetic doublets were fitted to each spectrum: two consistent with Fe^{3+} and one consistent with Fe^{2+}, using the Recoil analysis software package. Extracted Centre Shift (CS), Quadrupole Splitting (QS), half-width, half-height line width (LW) parameters and relative areas are provided in Table 2 and fitted spectra are shown in Fig. 4. The analysed iron redox ratio, $Fe^{2+}/\Sigma Fe$, is based on fitted peak areas, and we have assumed that the recoil-free fraction ratio $f(Fe^{3+})/f(Fe^{2+}) = 1.0$. In all four cases, fitting the single Fe^{2+} doublet was difficult owing to its weakness. Consequently, the fitted Fe^{2+} CS, QS and LW carry greater uncertainties than the two strong Fe^{3+} doublets.

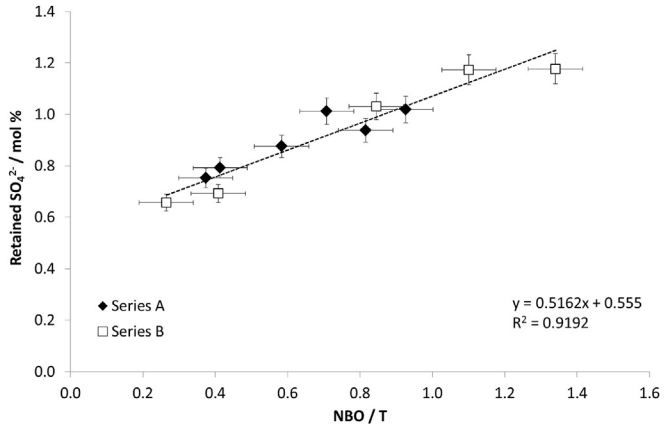

Fig. 3. Retained sulfate, SO_4^{2-}, as a function of non-bridging oxygen to tetrahedral ratio, NBO/T (excluding sulfate), for model glasses.

Laser Raman spectroscopy was carried out on as-poured samples using a Renishaw inVia spectrometer using a solid state 532 nm, 100 mW laser in back scattering geometry with a 50 cm^{-1} edge filter. Multiple spectra were measured and then summed for each sample at 20× magnification from 200 to 1500 cm^{-1} and recorded by a PC. Spectra are shown in Fig. 5 (Series A) and Fig. 6 (Series B).

3. Results

Analysed glass compositions are given in Table 1 and show considerable changes in sulfate content across a range of changing glass composition. Principally this is a result of changes in SiO_2 content and, as expected based on previous studies [18–21], sulfate content increases with decreasing SiO_2 content. However, changes in the proportions of the other constituents also arise making it necessary to a consider both glass composition and structure if accurate modelling of sulfate capacity is to be carried out. Figs. 1 and 2 show the analysed residual SO_4^{2-} in sample glasses as functions of total cation field strength index and theoretical optical basicity, respectively. Fig. 1 exhibits an inverse linear relationship between $\Sigma(z/a^2)$ and [SO_4^{2-}], with a high R^2 of 0.9502 for the linear fit to the data. Figs. 2 and 3 show linear relationships between Λ_{th} and [SO_4^{2-}], and NBO/T and [SO_4^{2-}], with closely similar R^2 of 0.9302 and 0.9192, respectively. These values of R^2 are contrasted against plots (not shown) of [SiO_2] vs. [SO_4^{2-}], which provides an inverse linear relationship with R^2 = 0.8418 with greater fit residuals; and [Na_2O] vs. [SO_4^{2-}], which provides a linear relationship with R^2 = 0.9435 (graph not shown). The high degree

Table 2
Fitted ^{57}Fe Mössbauer parameters for end-member model glasses A1, A6, B1 and B6.

Parameter	Glass A1	Glass A6	Glass B1	Glass B6
Centre shift (Fe^{3+}_A) ± 0.02/mm s^{-1}	0.27	0.25	0.27	0.25
Quadrupole splitting (Fe^{3+}_A) ± 0.02/mm s^{-1}	1.25	1.18	1.26	1.17
HWHM linewidth (Fe^{3+}_A) ± 0.02/mm s^{-1}	0.24	0.22	0.26	0.23
Area fraction (Fe^{3+}_A) ± 0.01	0.43	0.49	0.50	0.42
Centre shift (Fe^{3+}_B) ± 0.02/mm s^{-1}	0.28	0.27	0.28	0.25
Quadrupole splitting (Fe^{3+}_B) ± 0.02/mm s^{-1}	0.76	0.73	0.79	0.74
HWHM linewidth (Fe^{3+}_B) ± 0.02/mm s^{-1}	0.23	0.21	0.24	0.22
Area Fraction (Fe^{3+}_B) ± 0.01	0.55	0.51	0.48	0.56
Centre shift (Fe^{2+}) ± 0.04/mm s^{-1}	0.88	0.91	1.07	1.08
Quadrupole splitting (Fe^{2+}) ± 0.04/mm s^{-1}	2.35	2.32	1.95	1.96
HWHM linewidth (Fe^{2+}) ± 0.04/mm s^{-1}	0.19	0.10	0.13	0.10
Area fraction (Fe^{2+}) ± 0.01	0.02	0.01	0.02	0.01
Iron redox ratio $Fe^{2+}/\Sigma FE$ ± 0.02	0.02	0.01	0.02	0.01

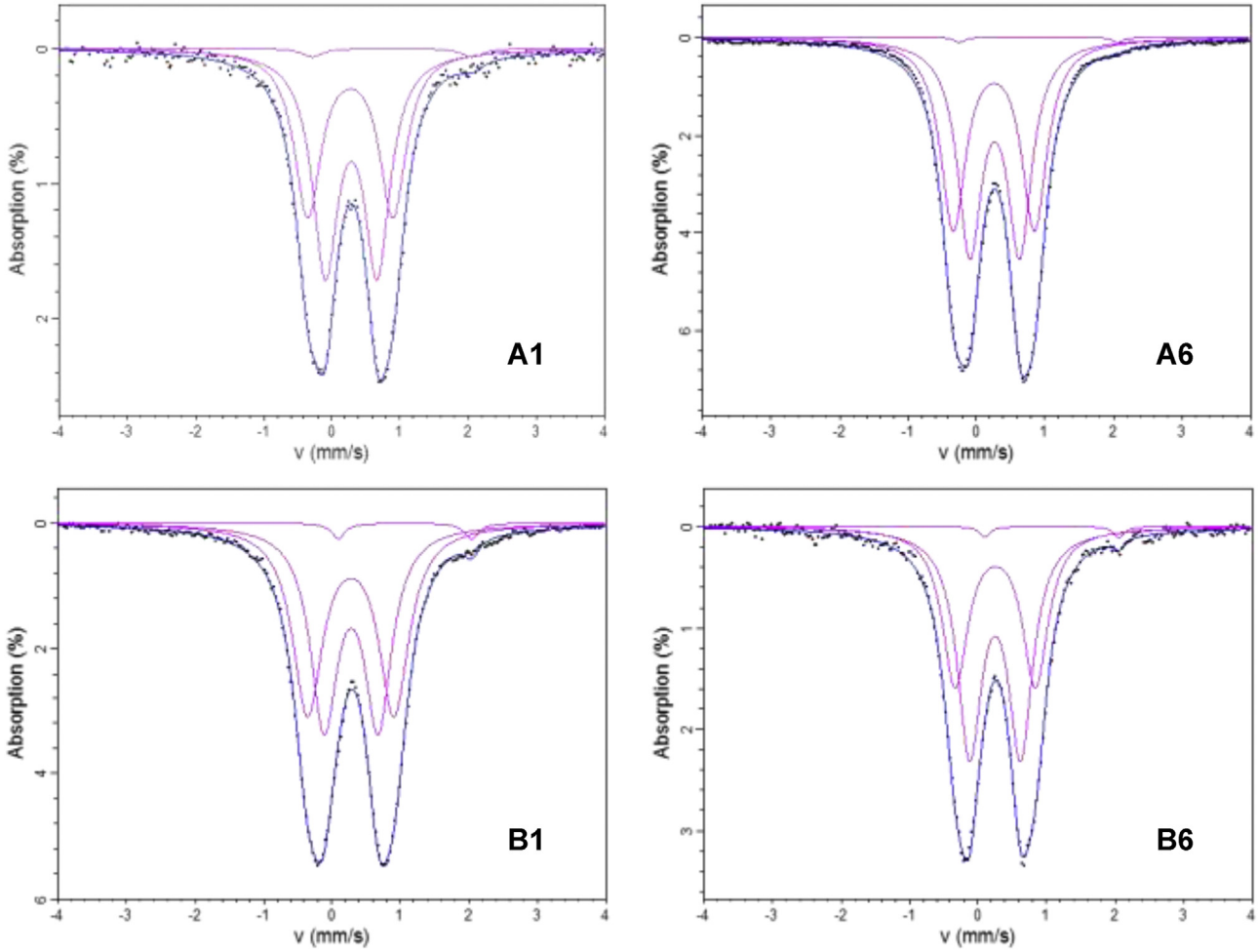

Fig. 4. Fitted ^{57}Fe Mössbauer spectra for end-member model glasses A1, A6, B1 and B6, showing two strong Lorentzian doublets attributed to $^{[4]}Fe^{3+}$ and one very weak Lorentzian doublet attributed to $^{[6]}Fe^{2+}$.

of correlation between sulfate capacity and Na_2O content is reflective of the limited range of glasses studied and in these glasses, the Na_2O content is a key driver of the depolymerisation of the network. Such simplistic models as [SiO_2] vs. [SO_4^{2-}] and [Na_2O] vs. [SO_4^{2-}] form useful guides, however, their limited applicability across a range of different glass compositions renders them less useful. More discriminating scales are needed and our results support the use of $\Sigma(z/a^2)$, Λ_{th} and NBO/T for this task. In particular, from the scales considered, $\Sigma(z/a^2)$ provides the best fit to the data.

^{57}Fe Mossbauer spectroscopy results, shown in Table 2 and Fig. 4, demonstrate that for all four samples the spectrum can be satisfactorily fitted by three broadened Lorentzian doublets. The hyperfine parameters (Table 2) for the weakest doublet (area 1–2%) are consistent with $^{[6]}Fe^{2+}$, whilst the hyperfine parameters for the two much stronger doublets are both consistent with $^{[4]}Fe^{3+}$.

From the Raman spectra a number of spectral differences can be observed through series A1 to A6 and B1 to B6 (wherein sample

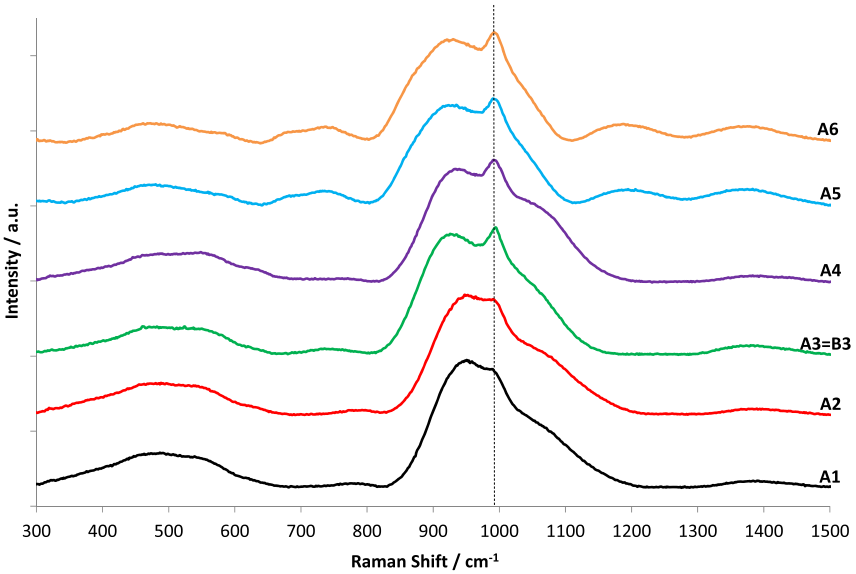

Fig. 5. Raman spectra for Series A model glasses. Dotted vertical line highlights peak at ~990 cm^{-1} in all spectra.

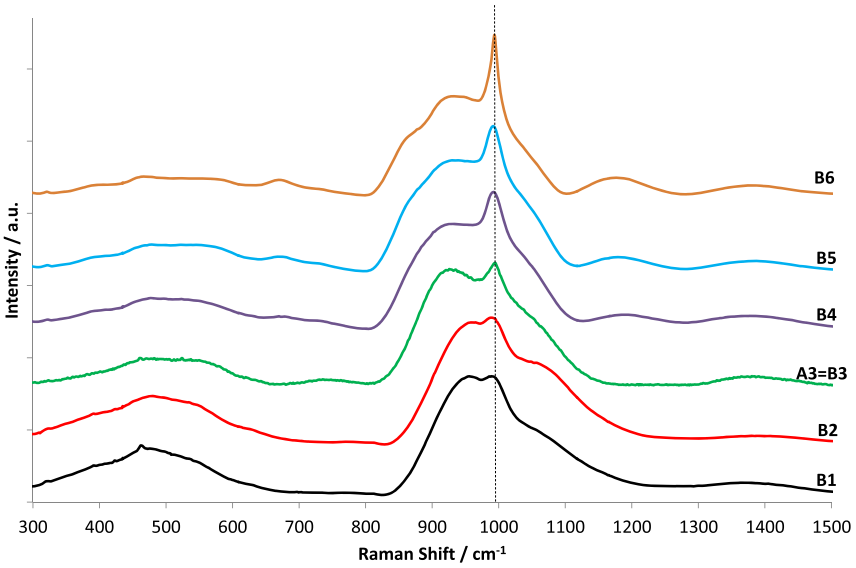

Fig. 6. Raman spectra for Series B model glasses. Dotted vertical line highlights peak at ~990 cm^{-1} in all spectra.

A3B3 is the centremost composition and common to both series), with a notable change between the groupings (A1–A4) and (A5–A6) and (B1–A3B3) and (B4–B6). Raman bands centred at approximately 460 cm^{-1}, 550 cm^{-1}, 630 cm^{-1}, 680 cm^{-1}, 740 cm^{-1} and 780 cm^{-1} dominate the lower-energy (300 - 800 cm^{-1}) regions of all spectra. The bands at 460 cm^{-1} and 550 cm^{-1} exhibit small changes, however, the weaker band at 630 cm^{-1} gradually disappears from A1 to A6. The bands at 680 cm^{-1} and 740 cm^{-1} are more prominent for samples A5 to A6 and B4 to B6. The higher-energy regions are dominated by broad, multi-featured bands between ca. 850 cm^{-1} and 1150 cm^{-1}, all with a notable and narrow band at 990 cm^{-1} which generally increases in intensity from A1 to A4, then maintains approximately the same intensity for A5 and A6; and which increases in intensity from B1 to B6. A broad band at 1375 cm^{-1} occurs for all samples, and a weak, broad band at 1200 cm^{-1} occurs for samples A5–A6 and B4–B6.

4. Discussion

Models describing the behaviour of sulfur in oxide melts have been developed and discussed over many years [4,6,10,19–21,55–58], and the reader is referred to those works and references therein for a wide-ranging treatment of the topic from waste vitrification, technological, and geological perspectives. For oxidised glasses and melts with direct applicability to radioactive waste vitrification, most recently a detailed empirical model for SO_3 capacity based on an analysis of over 250 data sets was developed by Vienna et al. [10]. This model is demonstrably applicable to current U.S. low-activity waste (LAW) glasses from the Hanford site and applies individual terms for many, but not all, glass components. Other models which are based on compositional and structural factors have been developed by Papadopoulos [55] and Ooura and Hanada [21], whose work informed modelling of sulfate

capacity in radioactive waste borosilicate glasses by Li et al. [56] and Liu et al. [57]. Also Jantzen et al. [6] developed a model based on viscosity (which is therefore related to composition and structure); and finally models from the geological and metallurgical literature which consider sulfur as S^{2-} are similarly based on composition/structure indicators [4,19,20,58]. Each model has its strengths, weaknesses and regions of validity. Most challenging of all has been demonstration and utilisation of any model across a sufficiently wide range of glass compositions as to render the model practically useful, yet there has been some success in this regard [6,10].

Previous work focussing on application of the cation field strength index model to the problem of sulfate capacity in radioactive waste glasses [4] demonstrated an inverse linear relationship between normalised (to 1 mol-cation) cation field strength index and log [SO_3], which provided the best fit to the data, measured in terms of R^2 ($\approx$0.84), for a wide range of phosphate glasses. The same relationship was also successfully applied to the borosilicate glass data of Lorier et al. [11] which, when considered independently, gave a high fit R^2 of 0.9779. When modelling the present data shown in Table 1 it was observed that, in terms of the fit R^2, a linear model of the plot of [SO_4^{2-}] vs. $\Sigma(z/a^2)$ as shown in Fig. 1, for which $R^2 = 0.9502$, was at least as good as a model, using the same model parameters as have been used throughout the present work, of log [SO_4^{2-}] vs. $\Sigma(z/a^2)$, for which $R^2 = 0.9497$ (not shown). In the light of this result a reappraisal of the previous fit in Ref. [4] to the borosilicate glass data of Lorier et al. [11] revealed that applying a linear model to [SO_4^{2-}] vs. $\Sigma(z/a^2)$ gave $R^2 = 0.9821$, which again is at least as good as the model to log [SO_4^{2-}] vs. $\Sigma(z/a^2)$, for which $R^2 = 0.9779$ as published in Ref. [4]. It is thus demonstrated that linear fits to [SO_4^{2-}] vs. $\Sigma(z/a^2)$ for both sets of data – from the present publication and from the Lorier fits in Ref. [4] – give no degradation of fit R^2 or significance, compared with fits to log [SO_4^{2-}] vs. $\Sigma(z/a^2)$. We therefore argue that the inverse linear relationship between [SO_4^{2-}] and $\Sigma(z/a^2)$ is also valid for the borosilicate glasses studied here and in Ref. [4]. The phosphate glasses surveyed in Ref. [4] covered a considerably wider compositional and structural envelope than the borosilicate glasses studied in Ref. [4] and here, and this may be one reason for the observed difference between the phosphate and borosilicate glasses. Re-modelling of the phosphate glass data from Ref. [4] with the models developed here produced the same trends in results as in Ref. [4], albeit with small differences in individual fit R^2 owing to careful selection of cation field strength and oxide basicity values, following the thorough survey of literature herein. The fits to the present data using the theoretical optical basicity scale, Λ_{th} (Fig. 2) also provide an R^2 value of 0.9302. This result is consistent with the previous results for phosphate glasses in Ref. [4], which also showed that $\Sigma(z/a^2)$ provided fits with higher R^2 compared with Λ_{th}. Nevertheless, the fits using Λ_{th} can still be considered to be good. The plot using NBO/T (Fig. 3) shows the same trend as the model using Λ_{th}, suggesting a degree of parity between these two scales in terms of their ability to accurately reflect the compositional and structural effects of the glass compositions studied here.

^{57}Fe Mossbauer spectroscopy results, given in Fig. 4 and Table 2, reveal that the iron in all samples studied is highly oxidised, with Fe^{3+} the overwhelming species in all cases. In all four samples the levels of Fe^{2+} were barely detectable, and account for only 1–2% of the total iron. This high level of oxidation is consistent with the presence of sulfate, which acts as an oxidising agent, and also with other results for laboratory-melted radioactive waste type alkali borosilicate glasses prepared under oxidising conditions [38,59,60]. Centre shift and quadrupole splitting values of the Lorentzian doublets fitted for Fe^{3+} are consistent with $^{[4]}Fe^{3+}$ [38,59–62]. Thus the combined CS, QS and redox information extracted from Mössbauer measurements confirm that, for the purposes of modelling cation field strength and optical basicity, the iron in the glasses studied here can be assumed to be present as $^{[4]}Fe^{3+}$.

Raman spectroscopy of Series A and B glasses, shown in Figs. 5 and 6 respectively, reveals highly convoluted spectra. This convolution arises from the presence of multiple Raman-active constituents and modes associated with network former - oxygen bonds such as Si-O and Al-O [63–66], referred to as T-O bonds [63]. Spectra also contain Fe-O [60], B-O and S-O [35,37,38,64–71] contributions. Le Losq et al. [63] distinguished Q^n species as tetrahedrally coordinated cations with n bridging oxygens (BO) and 4-n non-bridging oxygens (NBO). Crucially, they noted that Raman spectroscopy does not distinguish between Si- or Al- based tetrahedra, and the Raman signal of Q^n species mixes both SiO_4 and AlO_4 contributions. It may also include FeO_4 contributions. Furthermore, contributions from $^{[3]}B^{3+}$-O and $^{[4]}B^{3+}$-O groups, boroxyl rings and danburite/reedmergnerite groupings, can all occur in the same spectral range of ca. 600–1200 cm^{-1}. Any deconvolution of Raman spectra for such compositionally complex glasses as those studied here can provide multiple possible fits and attributions of individual peaks, and the lack of availability of accurate MAS-NMR data due to the presence of Fe^{3+} (see Section 2.1) further contributes to this. Consequently, we have considered and interpreted only the overall spectra here.

As summarised elsewhere [67–71] four vibrational modes of SO_4^{2-} tetrahedra arise in Raman spectra for sulfate in glasses, and are attributed as follows: ν_1 (symmetric S–O stretching modes) at ~ 990 cm^{-1}; ν_2 (symmetric O–S–O bending modes) at ~460 cm^{-1}; ν_3 (asymmetric S–O stretching modes) at ~1100 cm^{-1}; and ν_4 (asymmetric O–S–O bending modes) at ~ 620 cm^{-1}. The strongest of these bands, and the only one that can be clearly observed in the Raman spectra presented in Figs. 5 and 6, is the ν_1 symmetric S–O stretching band at ~990 cm^{-1}. The attribution of this mode to the observed band is further supported by the intensity of the band scaling qualitatively with the sulfate content of each glass, which is consistent with Lenoir et al. [68]. Intensity increases from Samples A1 to A4 (analysed SO_4^{2-} content increases from 0.75 to 1.01 mol %) and then it maintains approximately the same intensity for Samples A4, A5 and A6 (analysed SO_4^{2-} contents of 1.01, 0.94 and 1.02 mol %, respectively). For Series B glasses, intensity increases through Samples B1 to B6, with analysed SO_4^{2-} content increasing from 0.66 to 1.18 mol %. The Raman spectra therefore qualitatively support the analysed sulfate contents of each glass. There is no suggestion of lower oxidation of sulfur states than S(VI) in these glasses. The absence of Raman bands related to S-S bonds, S(IV) or S(V) complexes, which provide broad bands in the region 300–460 cm^{-1} [72,73] supports this. Further literature support for this conclusion is provided by X-Ray absorption spectroscopy for other sulfate-doped radioactive waste borosilicate glasses prepared under oxidising conditions [73] and from redox potentials [74], which show that lower sulfur oxidation states are not formed in glasses produced under oxidising conditions.

Raman spectroscopy also shows a change in the Q-speciation (Q^n) of Si-O bonds, with a gradual shift of the profile of the broad multi-component band at 850–1200 cm^{-1} towards lower Raman shifts. This is exemplified by the disappearance of the shoulder at ca. 1080 cm^{-1} and the growth of bands in the region of 850–950 cm^{-1}. This gradual decrease in average Q^n with decreasing SiO_2 content from A1 to A6 and B1 to B6 is consistent with results from many previous studies (see, for example, [60,63,64,66,68,71]). Raman bands in the region of 1200–1500 cm^{-1} have been attributed to BO_3 units [27,35,38,64,66]. Most of those studies which have considered Raman spectra above 1200 cm^{-1} concern glasses with B_2O_3 contents greater than ca. 15 mol%. Typically, spectra show only one broad band centred at ca. 1450–1500 cm^{-1}. However, Parkinson

et al. [75] also observed a band at ca. 1380 cm^{-1} for Fe_2O_3-doped SiO_2-B_2O_3-Li_2O-Na_2O glasses. Akagi et al. [76] also found a band at 1380 cm^{-1} for B_2O_3-K_2O glasses, attributing it to $BØ_2O^-$ triangles linked to $BØ_4^-$ units (where Ø = bridging oxygen atom). Few Raman studies of low-boron radioactive waste glasses have been published. For those which have [27,38,77], weak, broad bands at ca. 1200 cm^{-1} and/or 1380 cm^{-1} have been observed, as we have found in this study (Figs. 5 and 6). Both bands were attributed by those authors to BO_3 units [27,38,77]. It is noted that for samples A5 and A6, and B4, B5 and B6, an increase in intensity of the 1380 cm^{-1} band is accompanied by the emergence of bands at ca. 680 cm^{-1}, 750 cm^{-1} and 1200 cm^{-1}. Further study is required to fully understand the origins of these spectral changes, although results from other Raman studies of borate and borosilicate glasses [65,70] suggest that both $^{[3]}B^{3+}$ and $^{[4]}B^{3+}$ are involved. Raman evidence thus confirms the presence of $^{[3]}B^{3+}$ species in all glasses studied here, and it suggests that $^{[3]}B^{3+}$ makes up a major proportion of total boron, given the strength of the 1380 cm^{-1} band and the low (<8 mol%) total B_2O_3 contents of our glasses, although this is not proven. Raman evidence also suggests that the $^{[3]}B^{3+}/^{[4]}B^{3+}$ ratio may change through series A1–A6 and B1–B6. However, the lack of certainty over the structural origin of the band near 1200 cm^{-1} means that it is not feasible to quantify $^{[3]}B^{3+}/^{[4]}B^{3+}$ from Raman spectra.

Ooura & Hanada [21] studied sulfate solubilities of simple binary SiO_2-R_2O (R = Li, Na, K) and ternary SiO_2-Na_2O-R'O glasses (R' = Mg, Ca, Ba). For SiO_2-Na_2O glasses a strongly non-linear increase in sulfate capacity was observed with increasing Na_2O; this was related to the relative proportions of bridging oxygen (BO) and non-bridging oxygen (NBO) in the glass. Ooura and Hanada also stated that sulfate capacity in their SiO_2-R_2O glasses was independent of the nature of the alkali cation. However, we believe that their data does not fully support this particular conclusion for four reasons: (i) only data for one SiO_2-Li_2O and one SiO_2-K_2O glass were provided; (ii) analysed glass compositions were not provided - only sulfur contents were analysed using SEM-EDX analysis, and measurement uncertainties at low concentrations using SEM-EDX can be substantial; (iii) alkali volatilisation is known to increase with alkali cation size (Li < Na < K) and this could have affected final glass compositions, particularly given the small (5 g) melt size, thus affecting direct comparisons between glasses with nominally the same R_2O content; and (iv) their $75SiO_2$-$25Li_2O$ glass solubilised considerably more sulfate (ca. 2.7 mol% SO_3) than their $75SiO_2$-$25Na_2O$ glass (ca. 2.0 mol% SO_3). Considered cumulatively, we believe that there is insufficient data provided to fully support the conclusion in Ref. [21] that alkali type has no effect on sulfate capacity or solubility of SiO_2-R_2O glasses. Considering their SiO_2-Na_2O-R'O (R = Mg, Ca, Ba) glasses [21], sulfate capacity and solubility clearly increased in the order MgO < CaO < BaO for a given molar RO content and Na_2O as the alkali (therefore inter-sample differences in alkali volatility can reasonably be assumed to be small). The increases in sulfate capacity/solubility were linear with molar replacement of SiO_2 by RO, with the relationship displaying an increasing gradient in the order MgO < CaO < BaO. The data of Ooura and Hanada indicates additive effects of the content and nature of alkaline earth oxides on sulfate solubility. The cation field strength index model is qualitatively consistent with this result since it shows that all glass components play roles that are chemically and structurally unique, and therefore for a given molar concentration, each will have a unique effect on sulfate capacity and solubility. This is because each chemical element affects glass structure differently, in particular as functions of its concentration and chemical nature (charge, ionic radius, % ionic bond character and coordination). However, it is acknowledged that the cation field strength index and theoretical optical basicity scales do not provide single models which accurately describe all of Ooura and Hanada's data.

It has been suggested that sulfur solubility in oxide glasses can be predicted by combining the systemic acidity–basicity (measured by optical basicity) with a modified Toop-Samis polymeric model describing $[O^{2-}]$, the concentration of free oxygen ions; $[O^0]$, the concentration of bridging oxygen ions; and $[O^-]$, the concentration of non-bridging oxygen ions [58]. Such an approach considers the combined chemical (basicity) and structural (BO/NBO) effects which affect sulfur capacity and solubility in glass melts. As shown here and previously [4], a linear relationship is observed between the sulfate capacity and Λ_{th}. Cation field strength index can also represent chemical and structural factors in a single numerical scale and shows an inverse linear relationship with sulfate capacity. The results of the present study show enhanced performance of total cation field strength index normalised to 1 mol of oxide, compared with cation field strength index normalised to 1-mol-cation which was used previously [4]. As demonstrated by the high values of R^2 shown in Figs. 1–3, the cation field strength index, theoretical optical basicity and NBO/T scales can all be applied to sulfate capacity in borosilicate glasses for radioactive waste vitrification. Questions remain as to the limits of validity of this scale – for example composition, structure, temperature, redox conditions and melting time (i.e. equilibration time) will all affect the relationship. It is well known that sulfate solubility in oxide melts is highly sensitive to these parameters [4,17–20,55–58,68,69,73,74].

Differences are observed in R^2 between the fits to sulfate incorporation data using the cation field strength index, theoretical optical basicity and NBO/T scales. This raises the question of which scale is the most flexible, meaningful, accurate and/or precise. It is important to consider what each scale represents and how it is derived. The cation field strength is an arbitrary scale based on the electronic charge on a cation and the interatomic distance to its anion (in this case O^{2-}). Values can thus be obtained and are dependent on atomic charge and size, and consequently, may vary for a given cation in different oxidation states and coordination states. Theoretical optical basicity, Λ_{th}, is a measure of the electron donating power of constituent oxide ions in a glass. It expresses the ionic state of the oxide ion and represents the extent of negative charge residing on the oxygen ions. It has also been adapted and updated over the years by Duffy and other authors [50–54] to make provision for a wider range of cations in different coordination states and different host matrices. The ratio of non-bridging oxygens to tetrahedral species (NBO/T) is a measure of the theoretical proportion of non-bridging oxygens to the proportion of tetrahedrally-coordinated species. It is therefore essentially a measure of the degree of polymerisation of the glassy network. Whilst we have demonstrated here that it can be manipulated if cation environments are known or can be estimated, NBO/T makes no distinction between the effects of different glass modifiers or formers, for example between Li_2O, Na_2O and K_2O, and this could be considered a limitation. Optical basicity is primarily defined by charge, with space being fixed based on an arbitrary value although this can be controlled by using basicity moderating parameters for cations in different coordination states. Cation field strength, z/a^2, is defined by both cationic charge and ionic radius, and variations in either of these can be accommodated. Our view, based on the modelling of the glass composition – structure relationships considered here, is that because it can most readily accommodate changes in cation coordination, and because it has greater clarity in terms of the most appropriate z/a^2 values to use, the cation field strength scale is a particularly versatile and discriminating scale. Whilst theoretical optical basicity is, in many ways, equivalent to cation field strength index, multiple oxide basicity values are now

available for some oxides (see Refs. [50–54]) and selecting the most appropriate values to use for a model of a particular system is not always clear – this may be one reason why a higher R^2 is provided here by the fit cation field strength index (Fig. 1), compared with theoretical optical basicity (Fig. 2). As an example of the different accuracies/applicabilities of the three scales used here, the cation field strengths of $^{[3]}B^{3+}$ and $^{[4]}B^{3+}$ are respectively 1.622 and 1.407, the difference in values being due to different B^{3+} ionic radii in these coordinations. Coordination, as well as charge, affects the ability of any ion to accept or donate charge. The optical basicity scale provides a similar mechanism by which the basicity moderating parameter for B^{3+} can be selected if microscopic optical basicities [50] are known or used. However, as noted earlier, multiple values of the basicity moderating parameters have been published. The NBO/T scale can accommodate differing levels of $^{[3]}B^{3+}$ and $^{[4]}B^{3+}$, however, it does not discriminate between the effects of, for example, $^{[4]}B^{3+}$, Si^{4+} or P^{5+} and is based solely on their abundance. Consequently, the above factors may partly explain the observed fit R^2 values of $\Sigma(z/a^2) > \Lambda_{th} >$ NBO/T.

We will now consider the chemical/structural/physical origins of the observed sulfate capacities of the glasses studied. The question arises: why do lower cation field strength index, or higher optical basicity or NBO/T lead to higher levels of retained sulfate? In order for sulfate, SO_4^{2-}, to be incorporated into the glassy network as a tetrahedral unit, it requires charge compensation/stabilisation to provide local charge neutrality. It is widely accepted that this function is performed by glass modifiers, typically alkali or alkaline earth cations. Therefore, the amount of sulfate that can be incorporated in the glass is strongly dependent on the amount of network modifier present. However, other constituents such as B^{3+}, Al^{3+} and Fe^{3+} also require charge compensation/stabilisation for adoption of tetrahedral coordination, and the Q-speciation of the silicate network is also controlled by modifier type and content. Several authors have discussed the structural aspects of sulfate incorporation in oxide glasses [6,16–21,55–58], and the consensus is that the relationship between glass composition, glass structure and sulfate incorporation is controlled by the polymerisation of the network, and hence they are all related to the relative contents of BO, NBO and free oxygen. This topic was reviewed in depth to 2011 by Backnaes and Deubener [19]. However, it is clear from the findings of their review and also from the results presented here and elsewhere [10,21] that the nature of the modifier cations, as expressed by local bonding and space/charge effects, also plays a major role in sulfate incorporation. As discussed earlier, the results of Ooura and Hanada [21] show that, in the case of their SiO_2-Na_2O-RO glasses (R = Mg, Ca, Ba), increasing cation size (and hence decreasing z/a^2 and increasing Λ_{th}) of the alkaline earth cation led to a large increase in sulfate capacity for a given RO content such that Ba > Ca > Mg. However, the theoretical NBO/T at a given RO content for those glasses (Mg, Ca or Ba) is the same, irrespective of alkaline earth type. Backnaes and Deubener [19] noted that sulfate retention scales negatively with the cation field strength of alkaline earth metals, and that this may indicate that Q^n groups in different silicate melts are not energetically equivalent. They also argued that the abundance of free oxygen may not be the only structural parameter governing sulfate incorporation. Our results are consistent with this view. There is published data suggesting that sulfate capacity also scales positively with alkali type for borosilicate glasses, such that Li > Na > K [10], and also as discussed earlier, by Ooura and Hanada [21] for SiO_2-R_2O glasses where sulfate capacity may appear to scale Li > Na (although questions were noted over the accuracy of this data). Such behaviour, if it were shown to apply to the glasses studied here, is not consistent with the linear relationships demonstrated here using the $\Sigma(z/a^2)$ and Λ_{th} models (Figs. 1 and 2), as these indicate that alkalis should behave such that sulfate capacity scales Li < Na < K. Because understanding this particular behavioural aspect was not anticipated in the present study, the glass compositions we have studied here do not provide sufficient range of alkali types, contents and ratios to properly interrogate this hypothesis. However, it is possible to state that if the trends suggested above were shown to apply to radioactive waste type borosilicate glasses by interrogating robust data sets (e.g., from Ref. [10]), this in turn would suggest that the sulfate capacity of a ternary SiO_2-R_2O-R'O glass wherein R = Li, Na, K and R' = Mg, Ca, Ba would be greatest for SiO_2-Li_2O-BaO glasses and lowest for SiO_2-K_2O-MgO glasses with the same SiO_2, R_2O and RO contents. It is interesting to note that such a relationship was observed for stabilisation of $^{[4]}Fe^{3+}$ in SiO_2-R_2O-R'O glasses [78,79], and this may suggest a wider relationship between stabilisation/charge balance of some tetrahedrally-coordinated species in silicate glasses. It would also suggest a limitation of the applicability of the $\Sigma(z/a^2)$ and Λ_{th} scales for modelling sulfate capacities because they both indicate that alkali and alkaline earth metals should affect sulfate capacity in the same way, i.e., Li < Na < K and Mg < Ca < Ba. However, the results of Vienna et al. [10] were presented as a change in component content from centroid, in weight %, and therefore calculation and analysis of $\Sigma(z/a^2)$, Λ_{th} and NBO/T of the 253 glasses modelled in Ref. [10] would be required in order to make any comparisons robust. Considering this matter further, all three of the $\Sigma(z/a^2)$, Λ_{th} and NBO/T scales can be considered to present a cumulative representation of the chemical/structural nature of the glass, i.e. they do not provide the ability to accommodate for local inhomogeneities or the preference of any one cation (e.g., Na^+) or cation type (e.g., alkalis) to charge compensate or stabilise another cation in a particular coordination with respect to oxygen (e.g., $^{[4]}SO_4^{2-}$). It is important to consider any "preference" or "selectivity" of modifier cations to charge balance and stabilise $^{[4]}SO_4^{2-}$ over depolymerising the silicate network and providing NBO. Recent research by some of the present authors [80] has demonstrated that *pro rata* addition of SO_4^{2-} to binary SiO_2-Na_2O glasses close to the metasilicate composition has the effect of increasing average Si Q^n, i.e., polymerising the silicate network. This indicates that in these simple glasses SO_4^{2-} preferentially uses Na^+ for charge balance, thus leaving fewer Na^+ cations available to form NBO and thus provide depolymerisation of the silicate network. This is consistent with Tsujimura et al. [81], whose additions of Na_2SO_4 to SiO_2-Na_2O glasses led to little change in the Si Q^n compared with their SiO_2-Na_2O glasses with no additions of Na_2SO_4. Since the SO_4^{2-} was added as Na_2SO_4 in their case [81], the additional Na^+ charge-balanced the additional SO_4^{2-} in the glass. There is strong evidence that different modifier cations provide different Si Q^n at the same modifier content in silicate glasses. For example, the ^{29}Si MAS-NMR study of SiO_2-R_2O (R = Li, Na, K) glasses by Maekawa et al. [82] shows different Q^n distributions for given contents of Li, Na and K, across a range of alkali contents. The real effect may be even greater than they illustrated, since they used nominal and not analysed glass compositions in their calculations and it is established that alkali volatilisation during glass melting increases in the order Li < Na < K [42,83–85]. Therefore the real alkali contents of their glasses may have decreased in the order $Li_2O > Na_2O > K_2O$ for a given nominal alkali oxide content. In alkali borosilicate glasses doped with equimolar amounts of divalent cations, both the Q-speciation of silicon and the ratio of 3- to 4-coordinated boron, Si Q^n and N(B) respectively, have been shown to vary depending on the modifier cation type [86]. Connelly et al. [87] discussed the preference for charge compensation in silicate glasses and showed that this could be predicted using their bond valence model. However, their model did not include sulfate or different modifier cation types so it would require further development in order to apply it to the question of sulfate capacity.

Nevertheless, their work clearly demonstrates that preference for charge compensation takes place, and that it can be predicted for some glasses using their bond valence model.

It is also important to note that the effects of certain glass components are unlikely to be accurately modelled by any of the approaches considered here. These components include highly-charged cations such as V^{5+} and P^{5+}, for which empirical evidence shows that their incorporation can enhance sulfate capacities [10,67] and almost certainly sulfate solubilities. These constituents exhibit high cation field strengths, low basicities and are considered to be network-forming, so their addition would be expected to decrease sulfate solubilities according to the results of the three models ($\Sigma(z/a^2)$, Λ_{th} and NBO/T) considered here. In addition, other anionic species such as Cl^- are also known to reduce sulfate capacities [10] but they have not yet been assimilated into these models. Further work is required to establish the full ranges of applicability of these models to different glass systems; to glasses prepared under different conditions; and to a wider range of independent components. If, in the future, the model of Connelly et al. [87] can be extended and applied to these constituents it may shed new light on their behaviour. Clearly further study is required to more fully understand the effects, on a molecular basis, of alkali cation type on sulfate capacity in oxide glasses.

In terms of the present study, we can confidently conclude that the $\Sigma(z/a^2)$, Λ_{th} and NBO/T models can be applied to the problem of estimating trends in sulfate capacities of complex radioactive waste borosilicate glasses, *within the compositional and glass preparation envelopes considered here*. Whilst not being comprehensive sulfate capacity models, and having generated new research questions, our results support in particular the use of total cation field strength index, but also theoretical optical basicity and NBO/T models, to estimate trends in sulfate capacity. Consequently, this will enable reductions in the number of experimental glass melts that would be required to establish sulfate capacities within a given compositional envelope, and so these models can provide practical benefits in a range of applications.

5. Conclusions

Sulfate capacities of selected multicomponent borosilicate glasses representative of those used to vitrify high-level US radioactive wastes were studied as a function of glass composition. Raman spectroscopy showed decreasing average n in (Si Q^n) through two series of glasses, A1–A6 and B1–B6, and results were consistent with our attribution of a high proportion (67% of total boron) of $^{[3]}B^{3+}$. The characteristic ν_1 symmetric S–O stretching band at ~990 cm^{-1} scaled qualitatively with analysed sulfate content. ^{57}Fe Mössbauer spectroscopy confirmed that essentially all Fe was present in these glasses as $^{[4]}Fe^{3+}$. Sulfate capacity data for 11 glasses were accurately described by an inverse linear relationship between retained sulfate (SO_4^{2-}/mol %) and the total cation field strength index, $\Sigma(z/a^2)$, of the glass excluding the sulfate contribution, giving a very high goodness-of-fit, $R^2 \approx 0.950$. Linear relationships were also obtained using theoretical optical basicity, Λ_{th} ($R^2 \approx 0.930$) and NBO/T ($R^2 \approx 0.919$). Results support the use of $\Sigma(z/a^2)$, Λ_{th} and NBO/T for sulfate capacity modelling in the representative radioactive waste borosilicate glass compositions considered here, and they demonstrate a predictive method which could be used to accelerate the design and development of new glass compositions with enhanced or modified sulfate capacities.

Acknowledgements

The authors gratefully acknowledge funding from the U.S. Department of Energy – Office of Environmental Management via the International Cooperation Program. The authors also wish to thank Papken Hovsepian for help with some of the Raman measurements, and an anonymous reviewer for their insightful comments and suggestions.

References

[1] P. Sengupta, C.P. Kaushik, G.K. Dey, Immobilization of high-level nuclear wastes: the Indian scenario, Chapter 2, in: M. Ramkumar (Ed.), On a Sustainable Future of Earth's Natural Resources, Springer-Verlag, Berlin Heidelberg, 2013, pp. 25–51.
[2] I.W. Donald, B.L. Metcalfe, R.N.J. Taylor, J. Mater. Sci. 32 (1997) 5851–5887.
[3] O.J. McGann, P.A. Bingham, R.J. Hand, A.S. Gandy, M. Kavcic, M. Zitnik, K. Bucar, R. Edge, N.C. Hyatt, J. Nucl. Mater. 429 (2012) 353–367.
[4] P.A. Bingham, R.J. Hand, Mater. Res. Bull. 43 (2008) 1679–1693.
[5] W.K. Kot, H. Gan, I.L. Pegg, Ceram. Trans. 107 (2000) 441–449.
[6] C.M. Jantzen, M.E. Smith, D.K. Peeler, Ceram. Trans. 168 (2005) 141–152.
[7] P.A. Bingham, N.C. Hyatt, R.J. Hand, Glass Technol. Eur. J. Glass Sci. Technol. A 53 (2012) 83–100.
[8] P.A. Bingham, N.C. Hyatt, R.J. Hand, S.D. Forder, Glass Technol. Eur. J. Glass Sci. Technol. A 54 (2013) 1–19.
[9] A.L. Billings, K.M. Fox, Int. J. Appl. Glass Sci. 1 (2010) 388–400.
[10] J.D. Vienna, D.–S. Kim, I.S. Muller, G.F. Piepel, A.A. Kruger, J. Am. Ceram. Soc. 97 (2014) 3135–3142.
[11] T.H. Lorier, I.A. Reamer, R.J. Workman, Initial Sulfate Solubility Study for Sludge Batch 4 (SB4), SRNL Report WSRC-TR-2005–00213, 2005, http://sti.srs.gov/fulltext/2005/TR2005213.pdf.
[12] K.M. Fox, T.B. Edwards, D.K. Peeler, Sulfate Retention in High Level Waste (HLW) Sludge Batch 4 (SB4) Glasses: a Preliminary Assessment, SRNL Report SRNL-STI-2006–00038, 2006, http://sti.srs.gov/fulltext/WSRC-STI-2006-00038.pdf.
[13] A.L. Billings, K.M. Fox, Sulfate Solubility Limit Verification for DWPF Sludge Batch 7b, SRNL Report SRNL-STI-2011–00482, 2011, http://sti.srs.gov/fulltext/SRNL-STI-2011-00482.pdf.
[14] K.M. Fox, T.B. Edwards, Summary of FY11 Sulfate Retention Studies for Defense Waste Processing Facility Glass, SRNL Report SRNL-STI-2012–00152, 2012, http://sti.srs.gov/fulltext/SRNL-STI-2012-00152.pdf.
[15] K.S. Matlack, W. Kot, H. Gan, I.L. Pegg, Enhanced Sulfate Management in HLW Glass Formulations, VSL Report 12R-2540–1, ORP-53932, 2012, http://www.osti.gov/scitech/servlets/purl/1059479.
[16] R.K. Mishra, K.V. Sudarsan, P. Sengupta, R.K. Vatsa, A.V. Tyagi, C.P. Kaushik, D. Das, K. Raj, J. Am. Ceram. Soc. 91 (2008) 3903–3907.
[17] C.P. Kaushik, R.K. Mishra, P. Sengupta, A. Kumar, D. Das, G.B. Kale, K. Raj, J. Nucl. Mater. 358 (2006) 129–138.
[18] S. Nagashima, T. Katsura, Bull. Chem. Soc. Jpn. 46 (1973) 3099–3103.
[19] L. Backnaes, J. Deubener, Rev. Mineral. Geochem. 73 (2011) 143–165.
[20] D.R. Baker, R. Moretti, Rev. Mineral. Geochem. 73 (2011) 167–214.
[21] M. Ooura, T. Hanada, Glass Technol. 39 (1998) 68–73.
[22] K.M. Fox, J.C. Marra, Chemical Analysis of Simulated High Level Waste Glasses to Support Sulfate Solubility Modeling, Savannah River National Laboratory Report SRNL-STI-2014-00342, Revision 0, 2014, http://sti.srs.gov/fulltext/SRNL-STI-2014-00342.pdf.
[23] T. Jin, D. Kim, L.P. Darnell, B.L. Weese, N.L. Canfield, M. Bliss, J.R. Davies, C.C. Bonham, M.J. Schweiger, A.A. Kruger, in: Proc. Glass Opt. Mater. Div. Meeting, Amer. Ceram. Soc., Madison WI USA, 2450402, 2016.
[24] A. Dietzel, Glastech. Ber. 22 (1948) 41–49.
[25] A. Dietzel, Glastech. Ber. 22 (1948) 81–86.
[26] H.-I. Kim, J.C. Sur, S.K. Lee, Geochim. Cosmochim. Acta 173 (2016) 160–180.
[27] A. Goel, J.S. McCloy, C.F. Windisch Jr., B.J. Riley, M.J. Schweiger, C.P. Rodriguez, Int. J. Appl. Glass Sci. 4 (2013) 42–52.
[28] G.E. Brown, F. Farges, G. Calas, Rev. Mineral. 32 (1995) 317–410.
[29] T. Taniguchi, M. Okuno, T. Matsumoto, J. Non-Cryst. Solids 211 (1997) 56–63.
[30] L.G. Soltay, G.S. Henderson, Can. Mineral. 43 (2005) 1643–1651.
[31] W.J. Dell, P.J. Bray, S.Z. Xiao, J. Non-Cryst. Solids 58 (1983) 1–16.
[32] Y.H. Yun, P.J. Bray, J. Non-Cryst. Solids 27 (1978) 363–380.
[33] J. Wu, J.F. Stebbins, J. Non-Cryst. Solids 355 (2009) 556–562.
[34] K.A. Murphy, N.M. Washton, J.V. Ryan, C.G. Pantano, K.T. Mueller, J. Non-Cryst. Solids 369 (2013) 44–54.
[35] I. Bardez, D. Caurant, P. Loiseau, N. Baffier, J.L. Dussossoy, C. Gervais, F. Ribot, D.R. Neuville, Phys. Chem. Glas. 46 (2005) 320–329.
[36] Y. Tanaka, Y. Benino, T. Nanba, S. Sakida, Y. Miura, Phys. Chem. Glas. Eur. J. Glass Sci. Technol. B 50 (2009) 289–293.
[37] J. Wu, J.F. Stebbins, J. Non-Cryst. Solids 362 (2013) 73–81.
[38] J. McCloy, N. Washton, P. Gassman, J. Marcial, J. Weaver, R. Kukkadapu, J. Non-Cryst. Solids 409 (2015) 149–165.
[39] H.D. Schreiber, J. Non-Cryst. Solids 84 (1986) 129–141.
[40] D.A. McKeown, W.K. Kot, H. Gan, I.L. Pegg, J. Non-Cryst. Solids 328 (2003) 71–89.
[41] K. Shimoda, T. Nemoto, K. Saito, J. Phys. Chem. B 112 (2008) 6747–6752.
[42] M.B. Volf, Chemical Approach to Glasses, Elsevier, Amsterdam, 1984.
[43] F. Farges, J. Non-Cryst. Solids 244 (1999) 25–33.
[44] F. Farges, G.E. Brown, J.J. Rehr, Geochim. Cosmochim. Acta 60 (1996) 3023–3038.

[45] F. Farges, G.E. Brown, A. Navrotsky, H. Gan, J.J. Rehr, Geochim. Cosmochim. Acta 60 (1996) 3039–3053.
[46] F. Farges, C.W. Ponader, G.E. Brown, Geochim. Cosmochim. Acta 55 (1991) 1563–1574.
[47] A.J. Connelly, N.C. Hyatt, K.P. Travis, E.R. Maddrell, R.J. Short, J. Non-Cryst. Solids 357 (2011) 1647–1656.
[48] G. Mountjoy, J. Non-Cryst. Solids 353 (2007) 1849–1853.
[49] R.D. Shannon, Acta Cryst. A32 (1976) 751–767.
[50] J.A. Duffy, M.D. Ingram, J. Non-Cryst. Solids 21 (1976) 373–410.
[51] A. Lebouteiller, P. Courtine, J. Solid St. Chem. 137 (1998) 94–103.
[52] J.A. Duffy, Phys. Chem. Glas. 45 (2004) 322–327.
[53] J.A. Duffy, Phys. Chem. Glas. Eur. J. Glass Sci. Tech. B 47 (2006) 582–587.
[54] J.A. Duffy, J. Phys. Chem. A 110 (2006) 13245–13248.
[55] K. Papadopoulos, Phys. Chem. Glas. 14 (1973) 60–65.
[56] H. Li, P.R. Hrma, J.D. Vienna, Ceram. Trans. 119 (2000) 237–246.
[57] L.-J. Liu, J.-Y. Li, D.-S. Qie, J. Nucl. Radiochem 31 (2009) 114–120.
[58] R. Moretti, G. Ottonello, Geochim. Cosmochim. Acta 69 (2005) 801–823.
[59] N.J. Cassingham, P.A. Bingham, R.J. Hand, S.D. Forder, Phys. Chem. Glas. Eur. J. Glass Sci. Technol. A 49 (2008) 21–26.
[60] B. Cochain, D.R. Neuville, G.S. Henderson, C.A. McCammon, O. Pinet, P. Richet, J. Am. Ceram. Soc. 95 (2012) 962–971.
[61] M.D. Dyar, Am. Mineral. 70 (1985) 304–317.
[62] G. Tomandl, in: D.R. Uhlmann, N.J. Kriedl (Eds.), Chapter 5 in Glass: Science and Technology 4B, Academic Press, New York, 1990.
[63] C. Le Losq, D.R. Neuville, P. Florian, G.S. Henderson, D. Massiot, Geochim. Cosmochim. Acta 126 (2014) 495–517.
[64] W.L. Konijnendijk, J.M. Stevels, J. Non-Cryst. Solids 20 (1976) 193–224.
[65] H. Liu, M.M. Smedskjaer, H. Tao, L.R. Jensen, X. Zhao, Y. Yue, Phys. Chem. Chem. Phys. 18 (2016) 10887.
[66] F. Angeli, T. Charpentier, D. de Ligny, C. Cailleteau, J. Am. Ceram. Soc. 93 (2010) 2693–2704.
[67] D. Manara, A. Grandjean, O. Pinet, J.L. Dussossoy, D.R. Neuville, J. Non-Cryst. Solids 353 (2007) 12–23.
[68] M. Lenoir, A. Grandjean, S. Poissonet, D.R. Neuville, J. Non-Cryst. Solids 355 (2009) 1468–1473.
[69] D.A. McKeown, I.S. Muller, H. Gan, I.L. Pegg, C.A. Kendziora, J. Non-Cryst. Solids 288 (2001) 191–199.
[70] G.D. Chryssikos, E.I. Kamitsos, A.P. Patsis, J. Non-Cryst. Solids 202 (1996) 222–232.
[71] W.L. Konijnendijk, J.H.J.M. Buster, J. Non-Cryst. Solids 23 (1977) 401–418.
[72] T. Tsujimura, X. Xue, M. Kanzaki, M.J. Walter, Geochim. Cosmochim. Acta 68 (2004) 5081–5101.
[73] D.A. McKeown, I.S. Muller, H. Gan, I.L. Pegg, W.C. Stolte, J. Non-Cryst. Solids 333 (2004) 74–84.
[74] H.D. Schreiber, S.J. Kozak, P.G. Leonhard, K.K. McManus, Glastech. Ber. 60 (1987) 389–398.
[75] B.G. Parkinson, D. Holland, M.E. Smith, C. Larson, G. Doerr, M. Affatigato, S.A. Feller, A.P. Howes, C.R. Scales, J. Non-Cryst. Solids 354 (2008) 1936–1942.
[76] R. Akagi, N. Ohtori, N. Umesaki, J. Non-Cryst. Solids 293–295 (2001) 471–476.
[77] J.S. McCloy, C. Rodriguez, C. Windisch, C. Leslie, M.J. Schweiger, B.R. Riley, J.D. Vienna, Ceram. Trans. 222 (2010) 63–76.
[78] P.A. Bingham, J.M. Parker, T.M. Searle, J.M. Williams, I. Smith, C. R. Chim. 5 (2002) 787–796.
[79] P.A. Bingham, J.M. Parker, T.M. Searle, I. Smith, J. Non-Cryst. Solids 353 (2007) 2479–2494.
[80] S. Vaishnav, E. R. Barney, A. C. Hannon, S. D. Forder and P. A. Bingham, Manuscript in preparation.
[81] T. Tsujimura, X. Xue, M. Kanzaki, M.J. Walter, Geochim. Cosmochim. Acta 68 (2004) 5081–5101.
[82] H. Maekawa, T. Maekawa, K. Kawamura, T. Yokokawa, J. Non-Cryst. Solids 127 (1991) 53–64.
[83] E. Preston, W.E.S. Turner, J. Soc. Glass Technol. 16 (1932) 331–349.
[84] E. Preston, W.E.S. Turner, J. Soc. Glass Technol. 17 (1933) 122–144.
[85] E. Preston, W.E.S. Turner, J. Soc. Glass Technol. 18 (1934) 143–168.
[86] D. Holland, B.G. Parkinson, M.M. Islam, A. Duddridge, J.M. Roderick, A.P. Howes, C.R. Scales, Appl. Magn. Reson 32 (2007) 483–497.
[87] A.J. Connelly, N.C. Hyatt, K.P. Travis, R.J. Hand, E.R. Maddrell, Phys. Chem. Glas. Eur. J. Glass Sci. Tech. B 52 (2011) 64–67.